ELSEVIER

Materials Science and Engineering A 433 (2006) 269–278

MATERIALS SCIENCE & ENGINEERING A

www.elsevier.com/locate/msea

Effect of friction stir processing on the microstructure of cast A356 aluminum

Z.Y. Ma [a,b], S.R. Sharma [b], R.S. Mishra [b,*]

[a] *Institute of Metal Research, Chinese Academy of Sciences, Shenyang 110016, China*

[b] *Center for Friction Stir Processing, Department of Materials Science and Engineering, University of Missouri, Rolla, MO 65409, USA*

Received 26 July 2005; received in revised form 22 June 2006; accepted 22 June 2006

Abstract

Friction stir processing (FSP) was applied to cast A356 Al to modify the as-cast microstructure. FSP homogenizes and refines the cast microstructure, completely eliminates porosity, and creates a microstructure with fine Si particles (0.25–0.42 μm) distributed in a fine grain aluminum matrix (3–4 μm). Further, FSP parameters significantly influence microstructural development in the processed zone of cast A356 Al. Generally, higher tool rotation rate creates a more homogeneous microstructure. At lower tool rotation rates, a macroscopically visible banded structure characterized by a low density of coarse particles, was detected in the nugget zone. However, FSP parameters did not significantly influence the Al matrix grain size. The varied distribution pattern, size, and volume fraction of Si particles at different locations within the FSP zone indicates inhomogeneous material flow. A post-FSP T6 heat treatment did not alter the Si particle distribution, but did significantly coarsen the Si particles.
© 2006 Elsevier B.V. All rights reserved.

Keywords: Friction stir processing; A356; Microstructural modification; Casting

1. Introduction

Cast A356 Al is one of the most widely applied commercial Al–Si–Mg alloys in the aircraft and automotive industries because it has good castability [1] and can be strengthened by artificial aging [2–4]. However, the mechanical properties of A356 are significantly affected by microstructural features such as secondary dendrite arm spacing (SDAS) [5,6], microporosity [7,8], intermetallics [9], eutectic silicon particles [10,11], and heat treatments [2,12]. The as-cast microstructure of A356 is usually characterized by a coarse dendritic structure, non-uniformly distributed Si particles, and porosity [5–8,13–16]. These microstructural features limit the mechanical properties of cast alloys, in particular toughness and fatigue resistance.

Friction stir processing (FSP), a development based on friction stir welding (FSW) [17], is a new solid state processing technique for microstructural modification [18,19]. The basic concept of FSP is remarkably simple. A rotating tool with pin and shoulder is inserted into a single piece of material and traversed along the desired path to cover the region of interest. A volume of processed material is produced by material moved from the front to the back of the pin. During this process, the intense plastic deformation and thermal exposure the material undergoes, results in a significant evolution in the local microstructure. The characteristics of FSP have led to several applications for microstructural modification in metallic materials. First, FSP has been used to generate fine-grained microstructures amenable to high strain rate superplasticity [18–22]. For example, fine, equiaxed grains of 3.8 and 1.5 μm were created by FSP in commercial 7075Al and Al–4Mg–1Zr, respectively, thereby resulting in superplastic elongations >1250% at a high strain rates of 1×10^{-2} and $1 \times 10^{-1}\ s^{-1}$, respectively [20,21]. Second, FSP can be used to produce a surface composite on an aluminum substrate. A SiC–Al surface composite layer 50–200 μm in depth, with well-distributed SiC particles and excellent bonding with the aluminum substrate, was produced by FSP. This resulted in a significantly hardened surface layer [23]. Third, FSP can be used to homogenize the microstructure of nanophase aluminum alloys. Berbon et al. [24] demonstrated significantly improved microstructural homogeneity of a nanophase Al–10%Ti–2%Cu alloy having an excellent combination of very high strength and ductility. Fourth, FSP can be used to homogenize the microstructure of metal matrix composites. Spowart et al. [25] reported that FSP significantly improved the distribution of SiC particles of

* Corresponding author. Tel.: +1 573 341 6361; fax: +1 573 341 6934.
E-mail address: rsmishra@umr.edu (R.S. Mishra).

0921-5093/$ – see front matter © 2006 Elsevier B.V. All rights reserved.
doi:10.1016/j.msea.2006.06.099

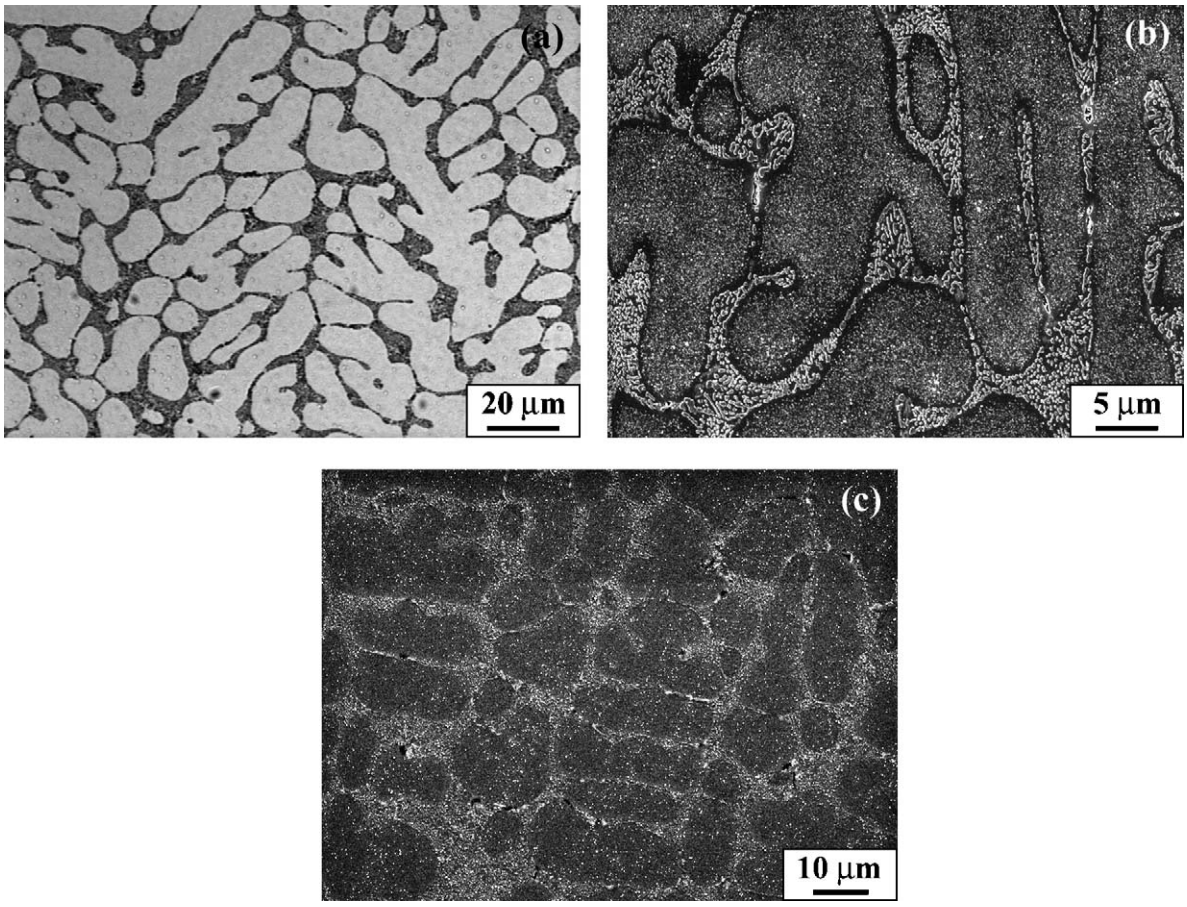

Fig. 1. Microstructure of as-received cast A356 Al: (a) dendritic structure (OM, as-polished); (b) interdendritic distribution of Si particles (SEM, slightly etched); (c) porosity between dendrites (SEM, as-polished).

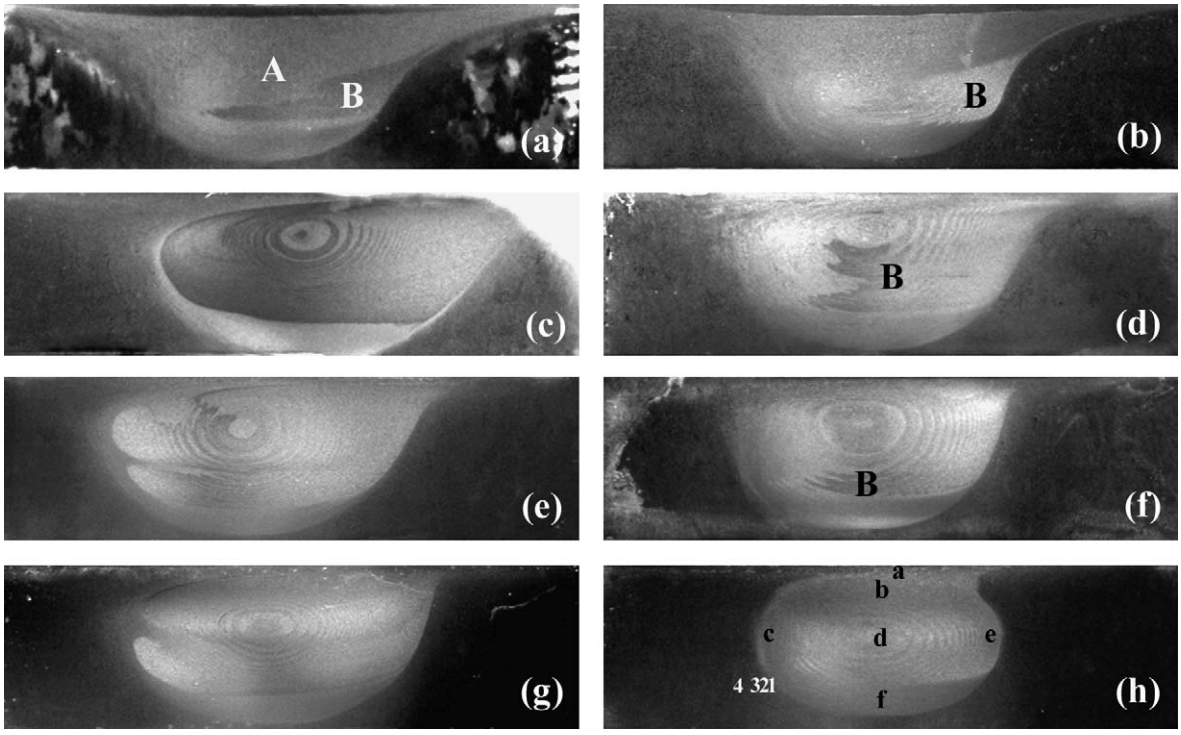

Fig. 2. Macrographs showing variation in the processed zone in FSP A356 samples with processing parameter combinations of (a) 300 rpm, 51 mm/min; (b) 300 rpm, 102 mm/min; (c) 500 rpm, 51 mm/min; (d) 500 rpm, 102 mm/min; (e) 700 rpm, 102 mm/min; (f) 700 rpm, 203 mm/min; (g) 900 rpm, 102 mm/min; (h) 900 rpm, 203 mm/min (samples were lightly etched). The advancing side of the nugget is on the right in all macrographs.

an as-extruded 6061Al-25v/o SiC_p composite, and ductility was thereby increased considerably.

Earlier we reported some preliminary results on the effect of FSP on the microstructure and mechanical properties of A356 Al [26,27]. Also, Santella et al. [28] have recently reported microstructural modification of cast aluminum alloys. FSP resulted in a remarkable homogenization and refinement of the cast microstructure and consequently the strength, ductility and fatigue properties improved significantly. In this study, the FSP samples were examined in detail microstructurally using both scanning and transmission electron microscopy (SEM and TEM), to understand the microstructural evolution during FSP.

2. Experimental approach

A commercial cast A356 Al billet with nominal composition 7.0%Si–0.3%Mg–bal Al (wt.%) was used. The casting method and temper condition of the as-received A356 casting were unknown to the authors. Single pass FSP was performed on 6.35 mm thick A356 monolithic plates machined from the as-received cast billets. Processing parameters used for FSP are summarized in Table 1. As-processed aluminum plates were cut transverse to the FSP direction, mounted, and mechanically polished. Keller's reagent was used to reveal microstructures. Microstructural examination was completed with optical microscopy (OM), scanning electron microscopy (JEOL T330A), and transmission electron microscopy (Philips EM430). Thin foils for TEM were prepared by ion thinning and jet polishing. Jet polishing was conducted at −25 °C using a solution 20%HNO_3 + 80%methanol (vol.%). The size and volume fraction of Si particles in various locations of the processed zone were estimated using Scion Image software.

Table 1
Summary of processing parameters for cast A356 Al

Tool rotation rate (rpm)	Tool traverse speed (mm/min)		
	51	102	203
300	x	x	–
500	x	x	–
700	–	x	x
900	–	x	x

To understand the effect of heat treatment on the microstructures of A356, both as-received and friction stir processed samples were subjected to a standard T6 heat treatment (solution-treated at 540 °C for 4 h, 25 °C water quenched, and then aged at 155 °C for 4 h) [29].

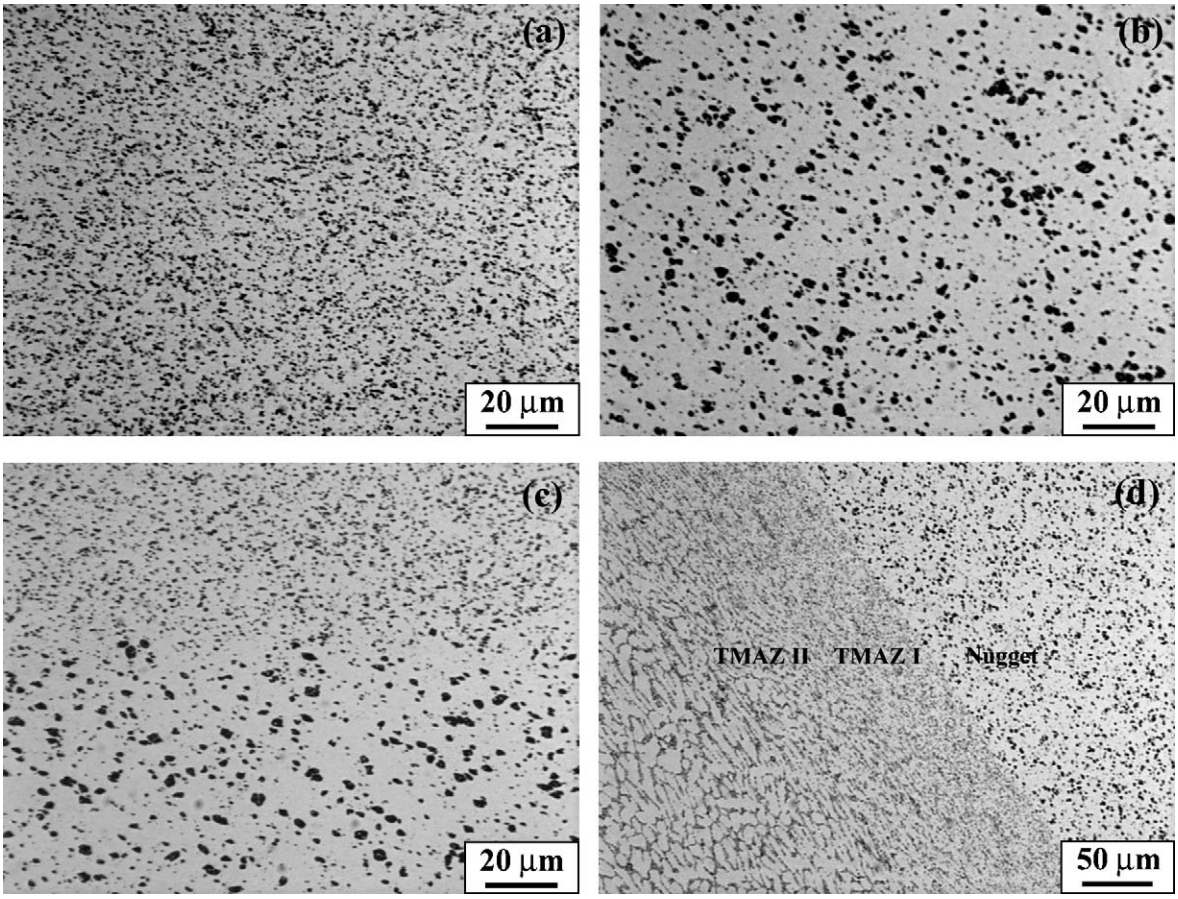

Fig. 3. Microstructure of polished as-FSP A356 sample (FSP parameter: 300 rpm, 51 mm/min): (a) fine Si particles in processed center (region A in Fig. 2a); (b) coarse Si particles in banded structure (region B in Fig. 2a); (c) boundary between fine-particle and coarse-particle zones; (d) transition zone between processed zone and parent metal of the FSP A356 sample.

3. Results

Fig. 1 shows optical micrographs of a polished A356 Al casting in the as-received condition. The microstructure of as-received A356 consists mainly of primary α-aluminum dendrites and interdendritic irregular Al–Si eutectic regions (Fig. 1a), i.e., the distribution of Si particles is not uniform throughout the aluminum matrix. While most Si particles exhibited a fibrous morphology, some had an equiaxed shape <1 μm in diameter (Fig. 1b). Generally, the as-received cast A356 Al plates showed a sound microstructure with relatively few pores 1–2 μm in diameter between the dendrites (Fig. 1c).

Fig. 2 shows macrographs of the friction-stir-processed zone. FSP parameters have a significant effect on the macrostructure as well as the microstructure in the stirred zone (hereafter referred to as the processed zone). The lower tool rotation rates (300–500 rpm) produced a basin-shaped nugget with a wide top region (Fig. 2a–d). With increasing tool rotation rate, the nugget changes from the basin shape to elliptical (Fig. 2e–h). At a tool rotation rate of 900 rpm and a traverse speed of 203 mm/min, an elliptical nugget with an onion ring structure was generated (Fig. 2h). There was a macroscopically visible banded structure (region B as shown in Fig. 2a, b, d and f) in the nugget zone for some parameter combinations. In some cases, the banded structure appeared to dominate the advancing side without appearing on the retreating side. At the lower rotation rate of 300 rpm, the banded structure exists for both traverse speeds of 51 and 102 mm/min (Fig. 2a and b). At the tool rotation rate of 500 rpm, while there was no banded structure for a tool traverse speed of 51 mm/min, it was detected for a traverse speed of 102 mm/min (Fig. 2c and d). For a constant traverse speed of 102 mm/min, increasing the tool rotation rate from 500 to 700 rpm eliminated the banded structure (Fig. 2d and e). However, at a constant tool rotation rate of 700 rpm, with an increase in the traverse speed from 102 to 203 mm/min, the banded structure appeared again (Fig. 2e and f). At the high rotation rate, the size of the banded structure was reduced considerably compared to that observed at lower tool rotation rates (Fig. 2f). For the highest rotation rate of 900 rpm, the banded structure was not detected in the nugget zone for traverse speeds of either 102 or 203 mm/min (Fig. 2g and h).

Optical microscopy revealed a high density of fine and nearly equiaxed Si particles uniformly distributed in most of the processed zone (Fig. 3a). However, the banded zone (region B in Fig. 2a, b, d and f) was characterized by a low density of coarse particles (Fig. 3b). These banded zones have distinct boundaries and good interface bonding (Fig. 3c). The particle size in the banded regions was significantly larger than in other regions of the processed zone. Fig. 3d shows the distinct microstructure at the boundary throughout the transition zone between the nugget and the parent metal on the retreating side. The microstructure changed from uniformly distributed Si particles in the processed zone to an ~60 μm wide thermo-mechanically affected zone (TMAZ I) of broken aluminum dendrites and Si particles distributed along upward flow lines. Within the TMAZ II, aluminum dendrites were deformed in an upward flow pattern, but not broken up.

By comparison, for the samples processed at higher tool rotation rates, the fine and equiaxed Si particles were uniformly distributed throughout the nugget zone. No coarse particles were detected (Fig. 4). The distribution of Si particles in this friction stir processed sample was significantly improved and porosity was completely eliminated compared to that in the as-cast sample (Fig. 4).

Fig. 5 shows the microstructure of the processed zone in various locations for the FSP A356 sample prepared at a tool rotation rate of 900 rpm and a traverse speed of 203 mm/min. While the Si particle distribution was random in the top and middle regions of the nugget (Fig. 5b and d), the Si particles exhibited somewhat directional distribution in the left, right, and bottom regions of the processed zone, i.e., a vertical distribution in the left and right regions and horizontal distribution in the bottom zone (Fig. 5c, e and f). However, the Si particle distribution in various locations was quite uniform, and no particle-rich or particle-free zones were detected. Si particle size in the left, bottom, and right regions of the nugget was smaller than that in the top and middle region, but the particle volume fraction for the former was higher than that for the latter. In a region above the processed zone (called a flow arm zone), coarse Si particles with low volume fraction were observed (Fig. 5a).

Fig. 6 shows the changing microstructure of the parent metal with increasing distance from the processed zone on the retreat-

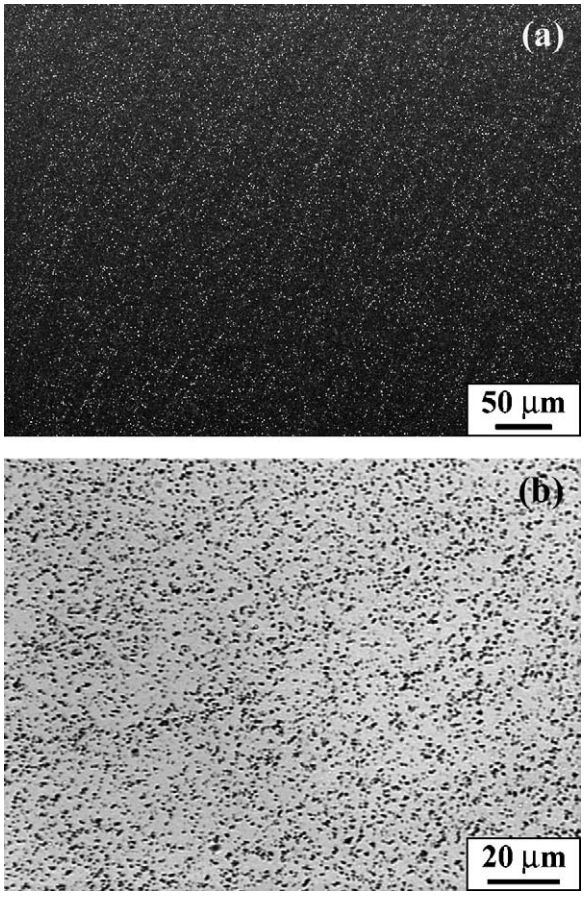

Fig. 4. Microstructure of polished as-FSP A356 sample (FSP parameter: 900 rpm, 203 mm/min): (a) SEM; (b) OM.

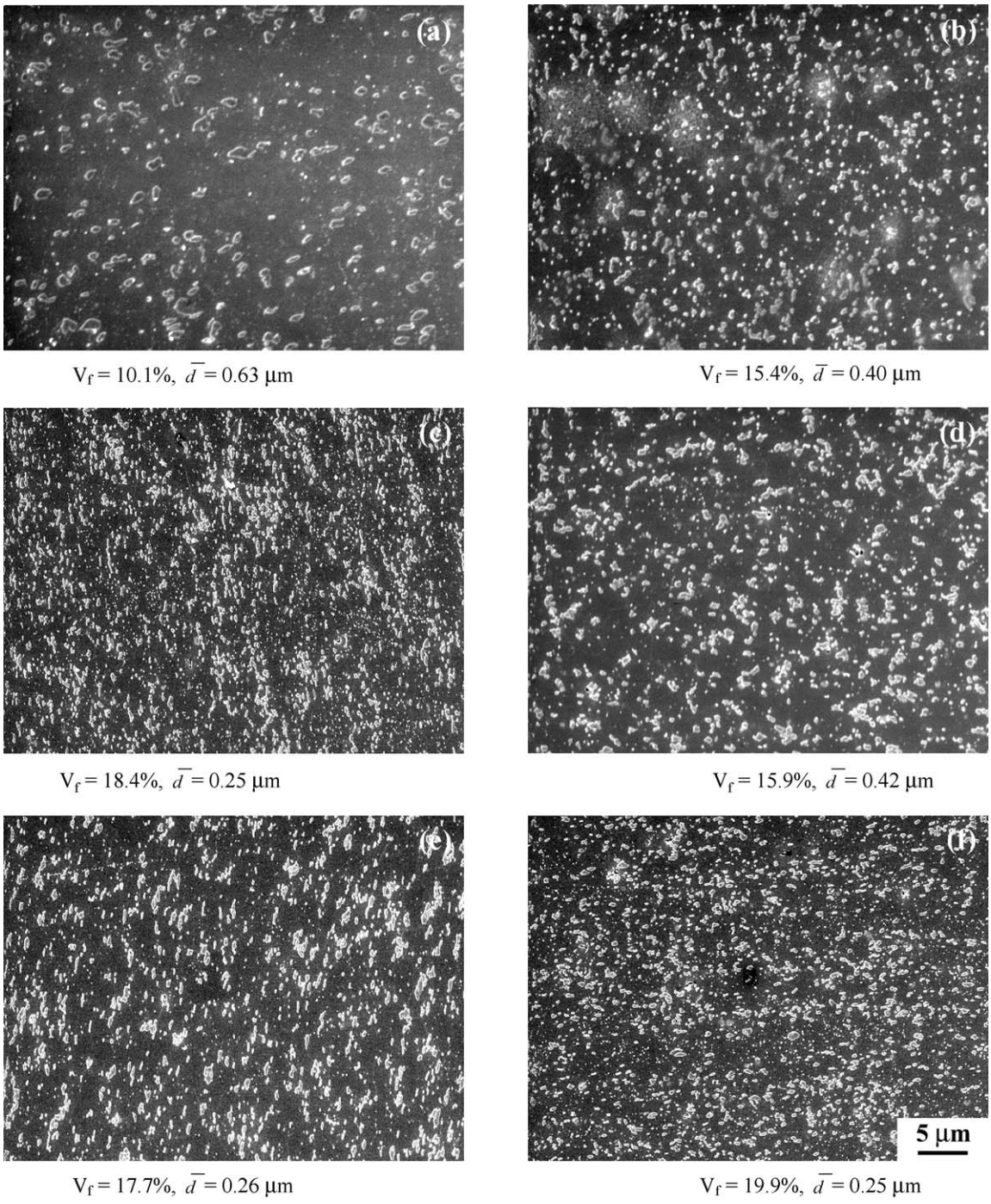

Fig. 5. SEM micrographs showing Si particle size and distribution in various regions of the processed zone of FSP A356 (FSP parameter: 900 rpm, 203 mm/min; sample was slightly etched): (a)–(f) correspond to locations a–f in Fig. 2h.

ing side. In a location very close to the processed zone boundary (Fig. 6a), the dendritic structure in the as-cast A356 alloy was completely broken up and the Si particles were generally distributed along upward flow lines. However, fibrous Si particles were not completely broken, and the size and distribution of Si particles were not uniform. In a location more distant from the processed zone (Fig. 6b), the dendrites were severely deformed, but not completely broken, and the interdendritic distribution of Si particles was still discernible. With increasing distance from the processed zone (Fig. 6c), the dendritic structure was deformed, but not broken up, and the interdendritic distribution of Si particles was distinctly seen. In a location far away from the processed zone (Fig. 6d), the microstructure remained as a typical dendritic structure as in the as-received casting.

Fig. 7 shows the microstructure of T6 heat-treated A356 Al samples. Compared to the as-received A356 Al casting (Fig. 1a), two observations can be made. First, the original aluminum dendrites isolated by the Al–Si eutectic regions became an interconnected aluminum matrix and individual aluminum dendrites were not readily discernible. Second, fibrous Si particles in the

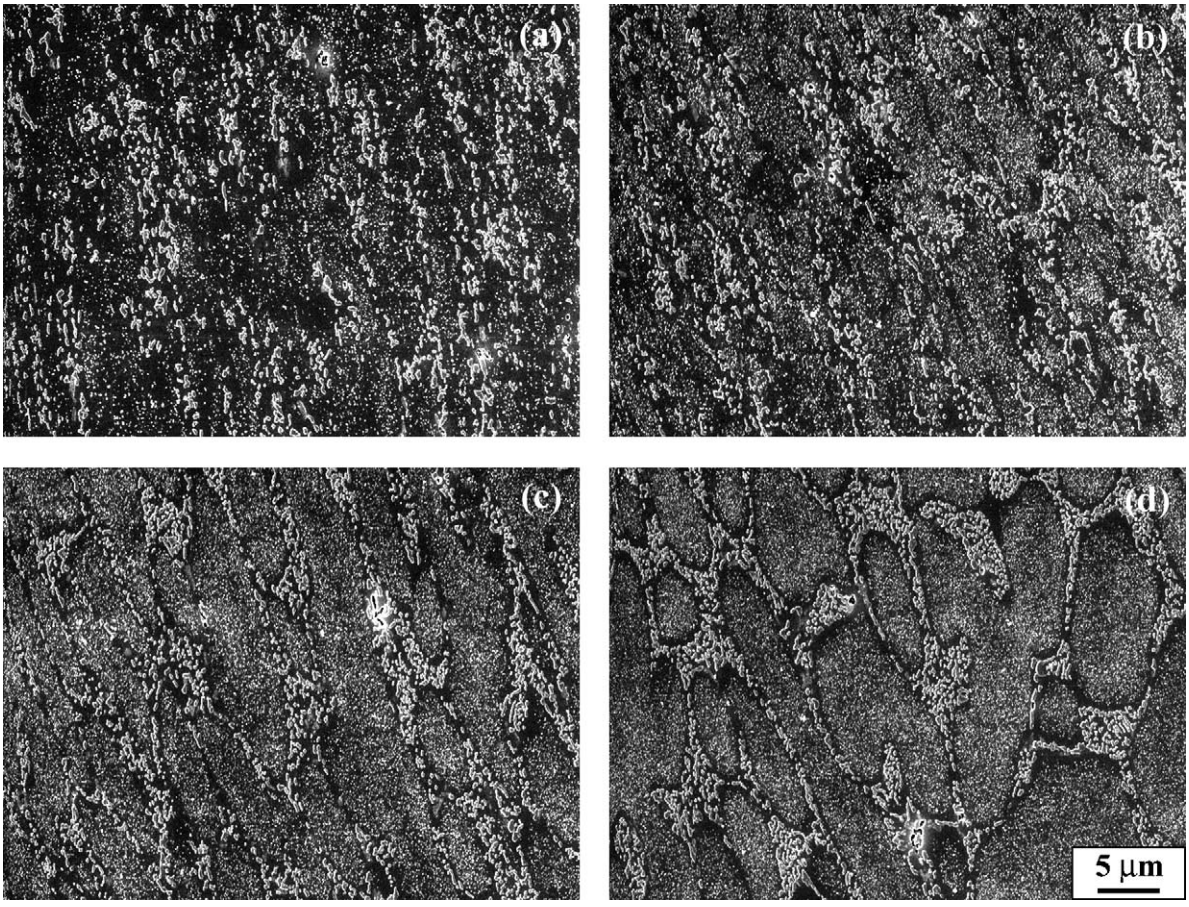

Fig. 6. SEM micrographs showing change in microstructure of parent material with increasing the distance from processed zone of FSP A356 (FSP parameter: 900 rpm, 203 mm/min; sample was lightly etched): (a)–(d) correspond to locations 1–4 in Fig. 2h.

as-received condition spheroidized completely and coarsened substantially, and were distributed along original aluminum dendrite boundaries as a chain (Fig. 7a). Furthermore, the interparticle spacing increased significantly. For friction stir processed samples, the T6-treatment did not change the distribution of Si particles, but resulted in substantial particle growth (compare Figs. 3a, 4b and 7b and c). For example, after the T6 heat-treatment, the average Si particle size at the center of friction stir processed zone, for a tool rotation rate of 900 rpm and a traverse speed of 203 mm/min, was estimated to be 0.89 μm. This is significantly larger than that in the as-FSP sample (0.42 μm at the nugget center).

Fig. 8 shows bright field TEM images of FSP A356 samples prepared at two processing parameters, i.e., 300 rpm at 51 mm/min and 900 rpm at 203 mm/min. Generally, grain boundaries in friction stir processed A356 are not easily distinguished. However, the grain size in both FSP A356 samples was estimated to be on the order of ~3–4 μm (Fig. 8a and c). Si particles were uniformly distributed both at grain boundaries and within the grains (Fig. 8b and d). While a certain amount of fibrous-like Si particles were still visible in the FSP A356 prepared at a tool rotation rate of 300 rpm and a traverse speed of 51 mm/min, the majority of Si particles exhibited an equiaxed morphology at a tool rotation rate of 900 rpm and a traverse speed of 203 mm/min (Fig. 8b and d).

4. Discussion

In cast Al–Si alloys modified by sodium or strontium, Si particles generally exhibit fibrous or equiaxed morphologies with fine size [30–32]. As shown in Fig. 1, the as-received A356 Al casting was characterized by a dendritic structure with fine Si particles having a fibrous and equiaxed shape distributed in the interdendritic region. This suggests that the as-received A356 casting was fully modified by sodium or strontium.

FSP resulted in a breakup of both the fibrous Si particles and the aluminum dendritic structure with a redistribution of Si particles in the aluminum matrix. FSP parameters exerted a significant effect on the stirred microstructure. At a low tool rotation rate of 300 rpm, the nugget zone of the samples did not exhibit an onion ring structure (Fig. 2a and b), as is often observed in transverse sections in FSW/FSP aluminum alloys [33–35]. With increasing tool rotation rate, the onion ring structure appears (Fig. 2c–h). At a high rotation rate of 900 rpm and high traverse speed of 203 mm/min, FSP generated the typical onion structure. Fig. 2 shows that some FSP parameter combinations created a banded structure in the processed zone. To provide insight into this phenomenon, the relationship between the presence of a banded structure and FSP parameters is plotted in Fig. 9 as rotation rate versus traverse speed. Two processing regions can be distinguished, i.e., one with a banded structure and another with-

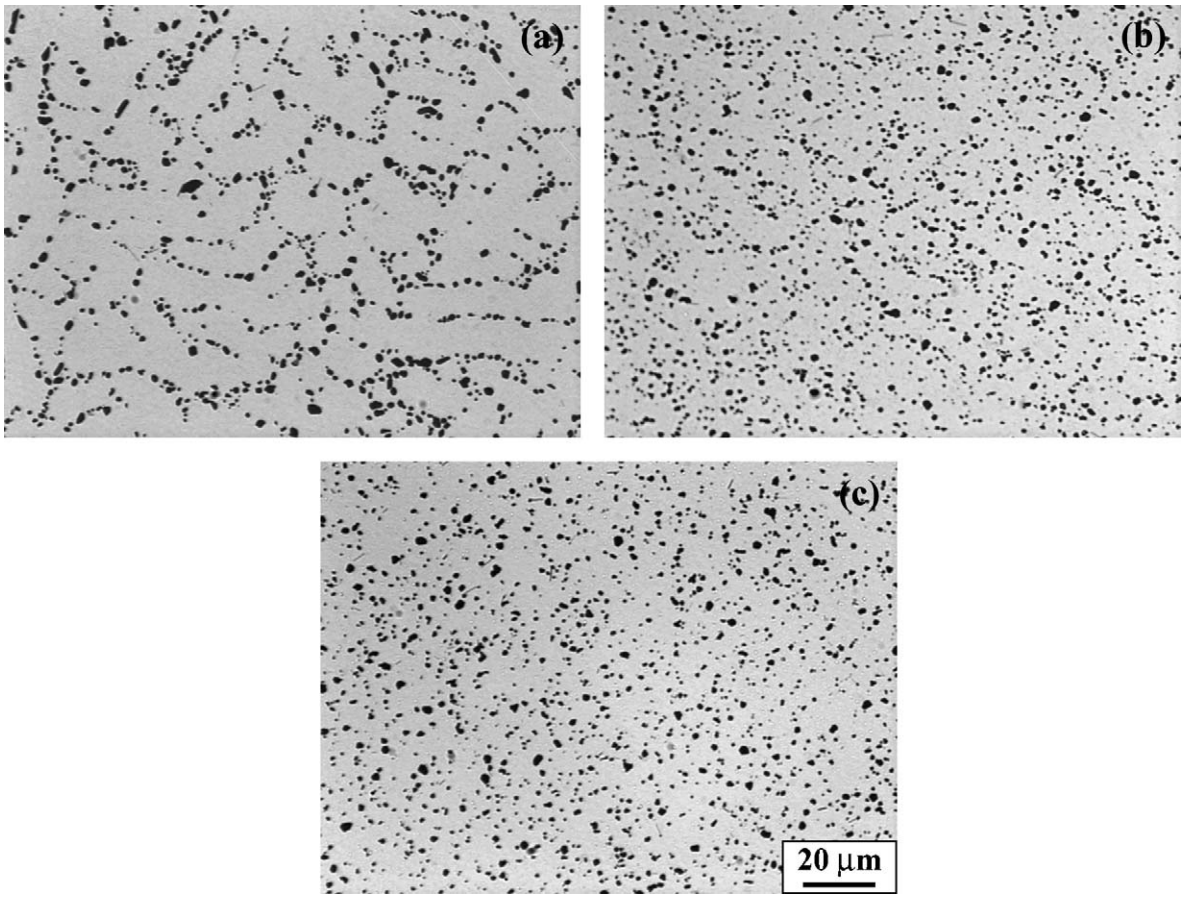

Fig. 7. Microstructure of polished T6-treated cast and FSP A356 samples: (a) cast alloy; (b) FSP alloy, 300 rpm, 51 mm/min (region A in Fig. 2a); (c) FSP alloy, 900 rpm, 203 mm/min.

out the banded structure. This plot shows that increasing either the tool rotation rate or rotation-rate/traverse-speed ratio leads to elimination of the banded structure. This is likely because a higher tool rotation rate intensifies frictional heating and stirring, creates a higher temperature in the stirred zone, and subsequently more thorough mixing of material and a more uniform distribution of Si particles. Fig. 3 shows that a banded structure is characterized by a low density of coarse Si particles. This indicates that lower tool rotation rates did not result in a complete dispersion of Si particles throughout the entire processed zone. By comparison, higher tool rotation rates did generate a uniform microstructure with fine Si particles (Fig. 4).

During solid solution treatment at high temperature (~540 °C), fibrous Si particles in the modified structure are fragmented and spheroidized much more rapidly than the plate-shaped Si particles in the unmodified structure [36,37]. Furthermore, such a treatment also led to significant coarsening of Si particles. Therefore, a T6 heat-treatment at 540 °C for 4 h resulted in significant spheroidization and coarsening of fibrous Si particles in the present A356 casting (Figs. 1a and 7a). Similarly, the T6 heat-treatment also resulted in significant coarsening of fine and equiaxed Si particles in the FSP A356 samples (Figs. 3a, 4b and 7b and c). The coarsening of Si particles results in an increase in the interparticle spacing in both cast and FSP A356 samples.

FSW/FSP results in the generation of a fine and recrystallized microstructure in aluminum alloys [18–22,35,38,39]. The grain size of ~3–4 μm in the present FSP A356 samples is in good agreement with that obtained in other FSW/FSP high-strength aluminum alloys [18–22,35,38,39]. Increasing the tool rotation rate or the tool rotation-rate/traverse-speed ratio resulted in increasing the grain size in the processed zone [20,38,40]. The present investigation shows that changing FSP parameters from 300 rpm at 51 mm/min to 900 rpm at 203 mm/min did not result in a significant change in grain size in the FSP A356 samples shown in Fig. 8a and c. The microstructure of the present modified A356 is different from that of high-strength aluminum alloys, with the modified A356 containing a high density of fine Si particles. Very likely the high density of fine Si particles in A356 exerted a significant effect on the recrystallization process and subsequent grain growth during the FSP thermal cycle, thereby influencing the eventual fine-grained structure. Fig. 8b and d show more fibrous Si particles in FSP A356 prepared at a low tool rate of 300 rpm than at a high tool rate of 900 rpm. This indicates that the high tool rotation rate better breaks up the Si particles and improves material mixing. This is consistent with the observations obtained by OM (Figs. 2–4).

Numerous investigations have been conducted to understand material flow behavior during FSW/FSP. A number of

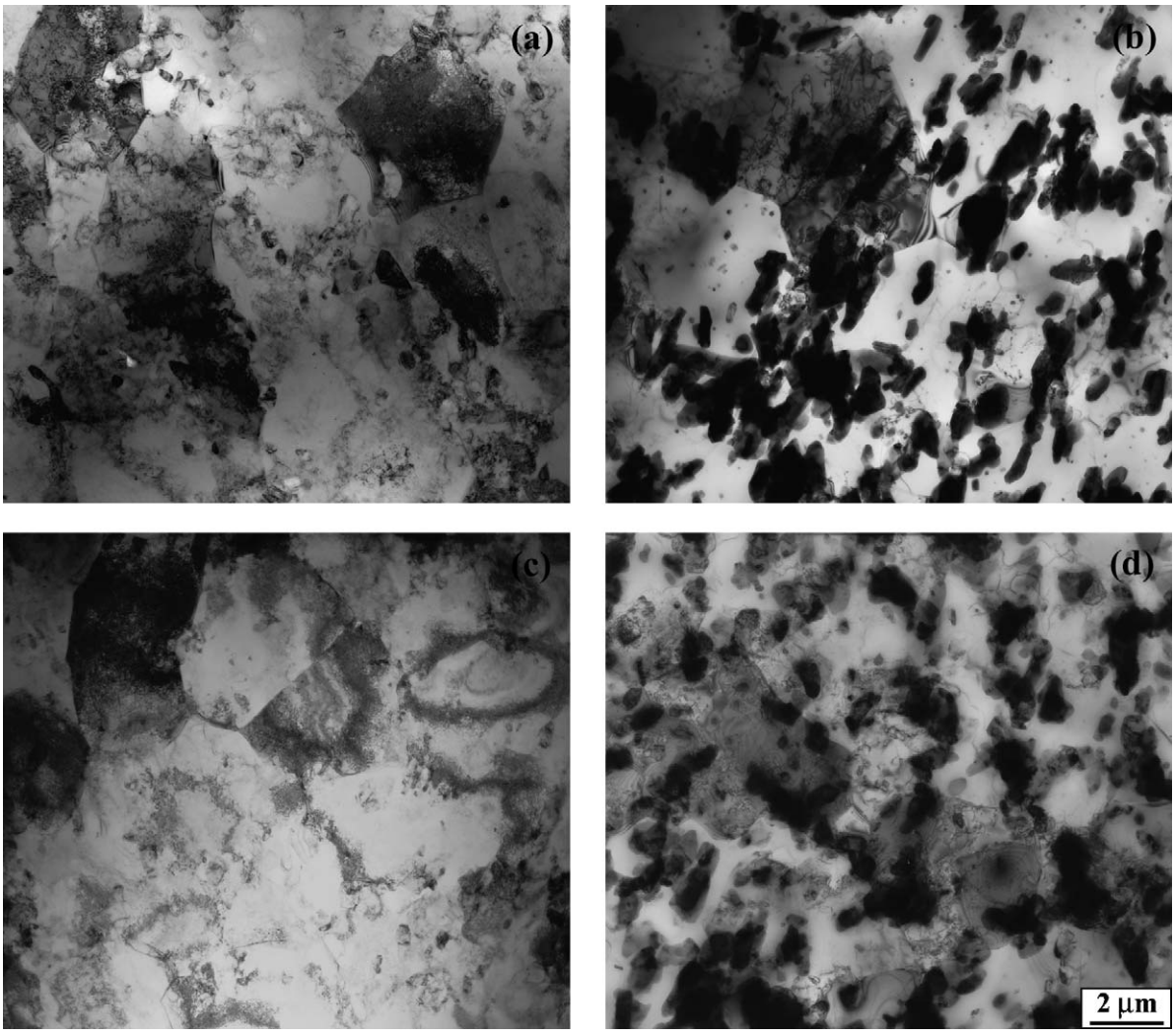

Fig. 8. TEM micrographs showing grains and Si particle distribution in FSP A356 samples prepared by (a and b) 300 rpm, 51 mm/min; (c and d) 900 rpm, 203 mm/min ((a) and (c) prepared by ion milling technique; (b) and (d) by jet polishing).

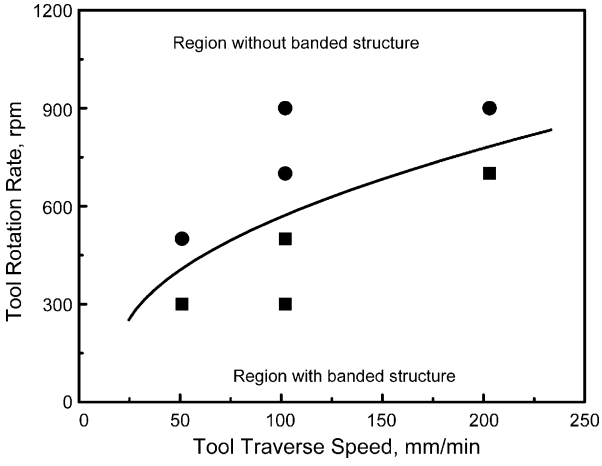

Fig. 9. Process map showing how FSP parameters influence the banded structure.

approaches, such as tracer techniques using markers and welding of dissimilar alloys/metals, have been tried to visualize material flow patterns in FSW [33–35,41–43]. However, the flow process of material during FSW/FSP is still not well-understood, and different explanations have been proposed. Krishnan [33], Reynolds et al. [41], and Colligan [42] suggested that FSW is similar to an extrusion process. During each tool rotation, a semicylindrical portion of the material is pushed to the back of the tool and around to the retreating side. A cross-sectional slice through such a set of semicylinders illustrates the onion ring structure often observed in traverse sections of the FSW/FSP nugget [33–35]. The "stirring" of material occurred only at the top of the weld where the material transport was directly influenced by the rotating tool shoulder that moved material from the retreating side around the pin to the advancing side [41,42]. In this case, there is very little material mixing during the FSW process. On the other hand, Biallas et al. [43] suggested that when the material flows around the pin within the plane of the sheet, it is reflected approximately at the imaginary walls of the groove that would be formed in the case of regular milling of

the metal. The induced circular movement leads to circles that decrease in radii and form the tube system. In this case, thorough mixing of material in the nugget region should occur.

The present study seems to indicate that FSP cannot be simply considered as an extrusion process, at least not in the conventional sense. This argument is based on the following considerations. First, an extrusion process cannot completely break up the dendrite structure in the cast A356 and transform a non-uniform distribution of particles into a very uniform distribution throughout the FSP zone. Second, at the lower tool rotation rate of 300 rpm, the nugget zone did not show an onion ring structure. Furthermore, a banded structure was observed in FSP samples prepared at several combinations of FSP parameters. This indicates that the material flow characteristics are significantly affected by the FSP parameters. Third, the varied distribution, size, and volume fraction of Si particles at various locations of the processed zone indicate different flow behaviors at various locations (Fig. 5). Fourth, the microstructural change in the TMAZs, with increasing the distance from the nugget zone, is difficult to explain by an extrusion process in the nugget zone (Fig. 6). The material flow behavior during FSW/FSP is complicated and depends on tool rotation rate and traverse speed.

5. Conclusions

(1) FSP resulted in the significant breakup of fibrous Si particle and aluminum dendrites and a redistribution of fine and equiaxed Si particles in the aluminum matrix.
(2) FSP resulted in generating fine grains of ∼3–4 μm in FSP A356 samples. FSP parameters did not exert a significant effect on the grain size.
(3) FSP parameters exert significant effects on the microstructure in the processed zone of a cast A356 alloy. Low tool rotation rates of 300–500 rpm resulted in creating basin-like processed zones; whereas at high tool rotation rates of 700–900 rpm, an elliptical processed zone with a typical onion ring structure was formed.
(4) A macroscopically visible banded structure was detected in the processed zone at lower tool rotation rates or lower rotation-rate/traverse-speed ratios. Such a banded structure was characterized by a low density of coarse Si particles. At higher tool rotation rates or higher rotation-rate/traverse-speed ratios, the banded structure disappeared and fine Si particles with a uniform size were homogenously distributed throughout the processed zone.
(5) Although the Si particle distribution in the processed zone is quite uniform for the FSP sample prepared at higher tool rotation rate of 900 rpm, the varied distribution pattern, size, and volume fraction of Si particles at various locations of the processed zone indicates different material flow characteristics.

Acknowledgments

The authors gratefully acknowledge the support of (a) the National Science Foundation through grant DMR-0076433 and the Missouri Research Board for the acquisition of a friction stir welding and processing machine, (b) DARPA for supporting this work under contract No. MDA972-02-C-0030, and to Mr. Murray Mahoney for review of this manuscript. Distribution Statement "A" (Approved for Public Release, Distribution Unlimited).

References

[1] D.L. Zalensas (Ed.), Aluminum Casting Technology, 2nd ed., AFS Inc., Illinois, 1993, p. 77.
[2] D.L. Zhang, L. Zheng, Metall. Mater. Trans. 27A (1996) 3983.
[3] T. Din, J. Campbell, Mater. Sci. Technol. 12 (1996) 644.
[4] Y.B. Yu, P.Y. Song, S.S. Kim, J.H. Lee, Scripta Mater. 41 (1999) 767.
[5] K. Radhakrishna, S. Seshan, M.R. Seshadri, AFS Trans. 88 (1980) 695.
[6] K.J. Oswalt, M.S. Misra, AFS Int. Cast Met. J. 6 (1981) 23.
[7] M.K. Surappa, E. Blank, J.C. Jaquet, Scripta Metall. 20 (1986) 1281.
[8] B. Closset, J.E. Gruzleski, Metall. Trans. 13A (1982) 945.
[9] G. Gustafsson, T. Thorvaldsson, G.L. Dunlop, Metall. Trans. 17A (1986) 45.
[10] C.H. Caceres, J.R. Griffiths, Acta Mater. 44 (1996) 25.
[11] Q.G. Wang, C.H. Caceres, Mater. Sci. Eng. A241 (1998) 72.
[12] C.H. Caceres, Q.G. Wang, AFS Trans. 104 (1996) 1039.
[13] S. Kumai, J. Hu, Y. Higo, S. Nunomura, Acta Mater. 44 (1996) 2249.
[14] B. Zhang, D.R. Poirier, W. Chen, Metall. Mater. Trans. 30 (1999) 2659.
[15] M.E. Seniw, J.G. Conley, M.E. Fine, Mater. Sci. Eng. A285 (2000) 43.
[16] G. Atxaga, A. Pelayo, A.M. Irisarri, Mater. Sci. Technol. 17 (2001) 446.
[17] W.M. Thomas, E.D. Nicholas, J.C. Needham, M.G. Murch, P. Templesmith, C.J. Dawes, G.B. Patent Application No, 9125978.8, December 1991.
[18] R.S. Mishra, M.W. Mahoney, S.X. McFadden, N.A. Mara, A.K. Mukherjee, Scripta Mater. 42 (2000) 163.
[19] R.S. Mishra, M.W. Mahoney, Mater. Sci. Forum 357–363 (2001) 507.
[20] Z.Y. Ma, R.S. Mishra, M.W. Mahoney, Acta Mater. 50 (2002) 4419.
[21] Z.Y. Ma, R.S. Mishra, M.W. Mahoney, R. Grimes, Mater. Sci. Eng. A351 (2003) 148.
[22] Z.Y. Ma, R.S. Mishra, Acta Mater. 51 (2003) 3551.
[23] R.S. Mishra, Z.Y. Ma, I. Charit, Mater. Sci. Eng. 341A (2003) 307.
[24] P.B. Berbon, W.H. Bingel, R.S. Mishra, C.C. Bampton, M.W. Mahoney, Scripta Mater. 44 (2001) 61.
[25] J.E. Spowart, Z.Y. Ma, R.S. Mishra, in: K.V. Jata, M.W. Mahoney, R.S. Mishra, S.L. Semiatin, T. Lienert (Eds.), Friction Stir Welding and Processing II, TMS, 2003, pp. 243–252.
[26] Z.Y. Ma, R.S. Mishra, M.W. Mahoney, in: K.V. Jata, M.W. Mahoney, R.S. Mishra, S.L. Semiatin, T. Lienert (Eds.), Friction Stir Welding and Processing II, TMS, 2003, pp. 221–230.
[27] S.R. Sharma, Z.Y. Ma, R.S. Mishra, Scripta Mater. 51 (2004) 237.
[28] M.L. Santella, T. Engstrom, D. Storjohann, T.-Y. Pan, Scripta Mater. 53 (2005) 201.
[29] H. Chandler (Ed.), Heat Treater's Guide—Practices and Procedures for Nonferrous Alloys, ASM International, Materials Park, Ohio, 1996, p. 257.
[30] K.T. Kashyap, S. Murrall, K.S. Raman, K.S.S. Murthy, Mater. Sci. Technol. 9 (1993) 189.
[31] L. Wang, S. Shivkumar, Z. Metallkd. 86 (1995) 441.
[32] D.L. Zhang, L.H. Zheng, D.H. StJohn, J. Light Met. 2 (2002) 27.
[33] K.N. Krishnan, Mater. Sci. Eng. A327 (2002) 246.
[34] W.D. Lockwood, B. Tomaz, A.P. Reynolds, Mater. Sci. Eng. A323 (2002) 348.
[35] M.W. Mahoney, C.G. Rhodes, J.G. Flintoff, R.A. Spurling, W.H. Bingel, Metall. Mater. Trans. 29 (1998) 1955.
[36] S. Shivkumar, S. Ricci Jr., C. Keller, D. Apelian, J. Heat Treat. 8 (1990) 63.
[37] S. Shivkumar, S. Ricci Jr., B. Steenhoff, D. Apelian, G. Sgiworth, AFS Trans. 97 (1989) 791.
[38] Y.J. Kwon, I. Shigematsu, N. Saito, Scripta Mater. 49 (2003) 785.

[39] K.A.A. Hassan, A.F. Norman, D.A. Price, P.B. Prangnell, Acta Mater. 51 (2003) 1923.
[40] H. Salem, A. Reynolds, J. Lyons, in: K. Jata, E.W. Lee, W. Frazier, N.J. Kim (Eds.), Lightweight Alloys for Aerospace Applications, TMS, Warrendale, PA, 2001, p. 141.
[41] A.P. Reynolds, T.U. Seidel, M. Simonnen, Visualization of material flow in an autogenous friction stir weld, Paper presented at First International Conference on Friction Stir Welds, Thousand Oaks, CA, USA, 1999.
[42] K. Colligan, Weld J. 78 (1999) 229S.
[43] G. Biallas, R. Braun, C.D. Donne, G. Staniek, W.A. Keysser, Mechanical properties and corrosion behavior of friction stir welded 2024-T6, Paper presented at First International Conference on Friction Stir Welds, Thousand Oaks, CA, USA, 1999.